Top-down synthesis of luminescent microplastics and nanoplastics by incorporation of upconverting nanoparticles for environmental assessment

Nadiia Yakovenko, Baptiste Amouroux, Magali Albignac, Fabrice Collin, Clément Roux, Anne-Françoise Mingotaud, Pierre Roblin, Christophe Coudret, Alexandra ter Halle

Top-Down Synthesis of Luminescent Microplastics and Nanoplastics by Incorporation of Upconverting Nanoparticles for Environmental Assessment

Received 00th January 20xx,

Accepted 00th January 20xx

DOI: 10.1039/x0xx00000x

Nadiia Yakovenko[a], Baptiste Amouroux[a], Magali Albignac[a], Fabrice Collin[a], Clément Roux[a], Anne-Françoise Mingotaud[a], Pierre Roblin[c], Christophe Coudret[a]*, Alexandra Ter-Halle[a]*

a : Laboratoire des IMRCP, Université de Toulouse, CNRS UMR 5623, Université Toulouse III - Paul Sabatier, Toulouse 31062, France E-mail: ter-halle@chimie.ups-tlse.fr (A. Ter-Halle), coudret@chimie.ups-tlse.fr (C. Coudret).

b : Laboratoire de Génie Chimique and Fédération de Recherche FERMAT, 31030 Toulouse, France.

Keywords: nanoplastic, UCNPs, lanthanide, powdering, milling, top-down synthesis, environmentally relevant, polymer

Abstract

The occurrence of micro- and nanoplastics is a major environmental problem. Especially for nanoplastics due to their easy bioavailability and unknown impact on living organisms. The monitoring of these extremely small particles during their ingestion, tissue translocation and transfer through the trophic chain remains very challenging. This study aims to develop an environmentally relevant model of luminescent micro- and nanoplastics. First, lanthanide-based upconverting nanophosphors (20 nm) were incorporated in bulk polyethylene without modification of the polymer structure or morphology. Second, micrometric and nanometric particles were obtained after powdering. Two fractions were obtained with cascade filtration

with average sizes of 5 µm and 150 nm and characterized in terms of size distribution, morphology and surface charge. The particles are very polydisperse with an irregular shape and a global negative charge; they exhibit morphological characteristics similar to those formed in the environment. Their luminescent properties upon NIR excitation at 980 nm open the possibility to track them in the tissues of organisms. The powdering method is very simple and compatible with many polymers pure or formulated. As a perspective, the use of weathered materials is possible with the proposed method and will allow the preparation of particles sharing additional properties with environmental micro- and nanoplastics.

Introduction

The scientific community has recently invested crucial effort in evaluating the impact of plastic on ecosystems, and this has allowed us to realize, in addition to the fact that all compartments of the earth were concerned, that the pollution reached the nanoscale. Our experience in engineered nanomaterials enables us to envisage that nanoplastics have unique physical and chemical properties (e.g., size, shape, composition, and reactivity). The very nature of nanoplastics (NPs, sizes are below 1 µm)[1-3] being polydisperse, polymorphic, and mainly made of C, H, and O, similar to natural organic matter, further complicates the analysis of NP behavior by traditional colloid science.

In recent decades, much attention has been given to the study of the occurrence and potential negative effects of microplastics (MPs, ranging from 1 µm to 5 mm).[4] MPs were analyzed in organisms ranging from zooplankton[5] to marine mammals.[6] Laboratory studies to investigate MP bioaccumulation and immunotoxicity in living organisms reported their biological impact on organisms (see references[7-9] for review). However, the fate and role of NPs remain poorly understood because of the lack of suitable analytical methods for monitoring their uptake, transport, and translocation and for understanding their potential adverse effects on living

organisms.[10] To date, most of the evaluation studies have been run on model NPs using commercially available polystyrene (PS) nanospheres.[11, 12] The distinction between model NPs and NPs—the nanoscale fraction of plastic debris generated in the environment—is often omitted even if their physicochemical and biological behavior are drastically different.[10] Model NPs are rather easy to handle and characterize but, lacking surface chemistry, polydispersity and an irregular shape similar to the one formed in the environment, they are of limited interest for ecotoxicological study.[10]

A few recent studies proposed a top-down approach (i.e., producing smaller particles from larger objects)[13] to prepare more environmentally relevant model NPs. Magrì et al. described the use of laser ablation in water to obtain polyethylene terephthalate nanoparticles with an average size of 100 nm and a surface chemical composition similar to plastic exposed to UV light in the environment.[14] Astner et al. produced model MPs and model NPs (in the range 360–390 nm) made of polybetaine adipate-coterephthalate and low-density polyethylene by applying a sequence mimicking environmental weathering.[15] El Hadri et al. produced NPs ranging from 20 nm to 1000 nm by applying blade grinding followed by planetary ball milling.[16] Model NP production from MPs collected in the environment was also proposed to prepare particles with a surface chemistry even closer to that of native nanoplastics. Their toxicological evaluation demonstrated that their impact on marine organisms was superior to that of PS nanospheres.[17] Even if the plastic particles obtained by the top-down methods reproduce the main physicochemical characteristics of NPs formed in the environment, their tracking remains challenging during biological evaluation tests, making it difficult to monitor their ingestion, transport, and translocation in living organisms.

Recent synthesis strategies, such as ^{13}C enrichment,[18] rare metals,[19] or simple staining methods with fluorescent dyes,[20] were used to obtain label model MPs and NPs. Fluorescence

78 labeling is a widely developed strategy, but most fluorescent tags operate with UV-blue to
79 green excitation light, showing low tissue penetration and toxicity to living organisms and
80 potentially leading to background autofluorescence, thus preventing their use in deep-tissue
81 imaging. Dyes can also suffer from photobleaching with prolonged exposures[21] or can have
82 solvatochromic properties, making the emission spectra dependent on the polarity of the
83 surrounding environment.[22] Another limitation is the potential costaining of the organic
84 matter present in the sample under focus, resulting in false detection. As an alternative to
85 fluorescence labeling, Mitrano et al. proposed the use of heavy metals as tracers and
86 inductively coupled plasma–mass spectrometry (ICP–MS) for indirect plastic monitoring.
87 Polyacrylonitrile particles doped with Pd were accurately assessed in a complex matrix
88 (activated sludge from wastewater treatment plant), and no Pd leaching from particles was
89 observed.[19] This strategy was found to be very efficient but is not well adapted for monitoring
90 MPs and NPs in living organisms because of the use of a destructive analytical technique.
91 The objective of the present study is to synthesize environmentally relevant models of MPs
92 and NPs in terms of polydispersity, shapes and surface properties that could be easily
93 visualized and tracked in the tissues of living organisms. Polyethylene (PE) was selected as a
94 model polymer because it is the most commonly used polymer and the most frequently found
95 polymer in the environment. However, especially at the nanoscale, this material is very
96 stealthy and poorly detectable using nondestructive methods. For easy imaging, lanthanide-
97 based upconverting particles (UCNPs) were incorporated into the polymer matrix. Because of
98 the spectroscopic features of the lanthanide family, these nanomaterials can accumulate
99 near-infrared (NIR) energy and release it as visible emission as a line spectrum typical of the
100 emitting element (thus erbium gives rise to a bright green visible emission).[23] They are
101 commonly used as background-free luminophores in imaging or anti-counterfeiting

applications[24] or as local sources of light ("nanolamps")[25] in material or biological applications.[26-29] Moreover, highly photostable (no blinking, no bleaching)[30] and requiring lower power density than 2-photon fluorophores, these background-free persistent fluorophores have become an attractive probe for imaging purposes, including thick samples. Furthermore, UCNPs derived from rare element salts ($NaREF_4$) can be prepared in a very monodispersed manner depending on the choice of rare earth elements and the preparation protocol. We chose to develop a top-down approach for the synthesis of labeled PE by incorporating highly monodispersed, hydrophobic and less than 30 nm UCNPs into bulk PE material and by using powdering to produce labeled nanometric particles with irregular shapes and a variety of sizes. The particles were characterized with many analytical techniques to obtain full information about their physicochemical properties.

Materials and methods

Chemicals: PE pellets (High-Density PE, CAS 9002-88-4) were purchased from Sigma Aldrich (Saint Louis, MO, USA). The polymer used was characterized by a melt flow index (MFI) of 12 g/10 min, a melting point between 125 and 140 °C and a density of 0.952 $g.mL^{-1}$ at 25 °C. Rare earth (RE) chloride hydrates, ammonium fluoride, oleic acid (OA) and 1-octadecene (ODE) were purchased from Alfa Aesar and used as received. All other organic solvents were of spectroscopic grade and used as received. Deionized water (ρ= 18 MΩ cm^{-1}) obtained from an Aquadem apparatus was used in this study.

Upconverting nanoparticle synthesis: In a three-necked flask, a solution of $YCl_3.6H_2O$ (2.4 g, 7.9 mmol), $YbCl_3.6H_2O$ (1.35 g, 3.5 mmol) and $ErCl_3.6H_2O$ (0.088 g, 0.23 mmol) in water (10 mL) was added to an OA:ODE mixture (35:190 mL:mL), and water was distilled off under an Ar flush. The resulting cloudy suspension was brought to 160 °C until clear (*ca* 1 h) and then

cooled under an Ar flush. NH_4F (2.37 g, 64 mmol, 80 mL, 0.8 M) and NaOH (1.86 g, 46.6 mmol, 80 mL, 0.58 M) were dissolved separately in MeOH. These two solutions were added simultaneously using syringe pumps at 0.4 $mL.min^{-1}$ to the vigorously stirred $RE(OA)_3$:OA:ODE solution. Once the addition was completed, the methanol was removed under an Ar flush at 100 °C. The reaction mixture, after careful degassing, was then brought to 310 °C as fast as possible (*ca* 20 $°C.min^{-1}$) and kept at this temperature for 90 min. After cooling, an equivalent amount of ethanol was added, and particles were collected by centrifugation at 9000 g for 10 min. They were purified by repeating twice the following sequence: pellet redissolution in cyclohexane/addition of the same volume of ethanol/centrifugation.

UCNP incorporation into PE : PE pellets were milled using a RETSCH ZM 200 ultracentrifugal mill. The obtained polymer powder with an average size of 200 µm was dissolved in boiling o-xylene (≥ 99.0% (GC grade); Sigma Aldrich, Saint Louis, MO, USA), where UCNPs (10 wt.% PE) were subsequently introduced. The mixture was homogenized by magnetic stirring at 146 °C for 20 min. Precipitation of the synthesized polymer material was achieved by rapid cooling in an ice bath. UCNPs that were not incorporated into PE were removed by washing the polymer with cyclohexane (≥99.7% (HPLC grade); Sigma Aldrich, Saint Louis, MO, USA). Before future use, the polymer was dried overnight at 40 °C. As a negative control, a second batch of polymers containing only PE (Blank-PE) was prepared following a similar protocol.

Synthesis of the labelled micro- and nanoparticles: Bulk materials Blank-PE and Upcon-PE were exposed to a cryogenic grinder (SPEX™ SamplePrep 6775 Freezer/Mill™, Delta Labo, Avignon, France). First, samples were precooled for 5 min, and then grinding was carried out in 10 cycles of 1 min with cooling between cycles for 2 min in liquid nitrogen. The grinding rate was 10 coups per second (CPS). The obtained polymer powder was dispersed in ethanol (≥99.8% (HPLC grade); Sigma Aldrich, Saint Louis, MO, USA) and sonicated for 15 min at room

temperature to avoid particle aggregation. Then, particle size separation was performed in 6 sequential filtration steps through a metal mesh with a cutoff of 500 µm (Retsch, Haan, Germany) and NITEX nylon mesh (Dominique Dutscher SAS, Brumath, France), with pore sizes of 200 µm, 100 µm, 50 µm, 11 µm, and 1 µm. Wet milling was performed in a 20 mL glass vial filled with approximately 50 g of ZY-E (yttrium stabilized zirconium oxide) beads, 1.0–1.2 mm (Sigmund Lindner GmbH (SiLi), Warmensteinach, Germany), 0.1 to 0.5 g of MPs, and approximately 10 mL of absolute ethanol. The milling process lasted 48, 60, and 120 days under 80 rpm stirring on a horizontal ROLLER 6 digital apparatus (IKA, Staufen, Germany). Eventually, MPs and NPs were separated by the 6 steps of subsequent filtration described above and rinsed with cyclohexane.

Granulometry analysis: The MP size distribution was determined using a Mastersizer MS3000 (Malvern Panalytical, UK). The polymer powder was dispersed in ethanol using a HYDRO MV device with stirring at 2500 rpm. The refractive indices used for ethanol and particles were 1.36 and 1.52, respectively, with an absorption index for particles of 0.1. The results are presented as the mean number of particles obtained from 5 measurements.

Differential scanning calorimetry: DSC was performed with a DSC1 Mettler Toledo apparatus equipped with an HSS8 sensor. Samples were weighed (between 5 and 7 mg) and sealed in 40 mL aluminum pans. They were heated from 20 °C to 160 °C at 5 °C/min with an empty aluminum pan as the reference. Dry nitrogen with a flow rate set at 20 mL/min was used as the purge gas. Each sample was analyzed in triplicate. The first heating cycle was used to erase all processing, thermal, mechanical, crystallization, and shear history of the samples. The melting temperature and crystallinity were obtained from the second heating cycle. The crystallinity was calculated from the expression:

$$\text{Crystallinity (\%)} = (\Delta H_m / \Delta H_{mref}) * 100 \quad (1)$$

where ΔH_m is the melting enthalpy of the analyzed samples, and ΔH_{mref} is the melting enthalpy of 100% crystalline PE (293 J/g).

Small-angle X-ray scattering (SAXS) analysis: SAXS measurements were performed on a XEUSS 2.0 laboratory source equipped with a PILATUS 1 M pixel detector (DECTRIS) and an X-ray source provided by a GeniX3D with a fixed wavelength based on Cu Kα radiation (λ = 1.54 Å). The distance between the sample and the detector was fixed at 1216.5 mm, giving a *q* range starting from 0.005 $Å^{-1}$ to 0.5 $Å^{-1}$, assuming that *q* is the scattering vector equal to $4\pi/(\lambda \times \sin\theta)$ with a 2θ scattering angle. The distance was calibrated in the small-angle region using silver behenate (d_{001} = 58.34 Å). For solid samples, the dry MP powder was placed between two Kapton windows with 1 mm of the optical pathway and placed on the motorized sample holder. For liquid samples, particle dispersion was injected into a capillary tube with a diameter of 1.5 mm and then placed under the beam in the conditions. To remove scattering and absorption from air, a primary vacuum was applied to the entire instrument. To maximize the signal at high angles, 6 acquisitions of 600 seconds were averaged. All scattering curves were corrected for the empty cell contribution or for the solvent, divided by the transmission factor, acquisition time and optical path to obtain SAXS curves in absolute units (cm^{-1}).

Transmission electron microscopy energy-dispersive X-ray spectroscopy: NP dispersions in ethanol were prepared with polyvinylpyrrolidone (PVP) 0.4% (w/v) to ensure particle adhesion on the top of the formvar/carbon-coated copper grid. One drop of 20 µL of sample solution was placed on the top of the grid. After drying, TEM/EDX analysis was performed using a JEOL cold-FEG JEM-ARM200F operated at 200 kV equipped with a probe Cs corrector reaching a spatial resolution of 0.078 nm. EDX spectra were recorded on a JEOL CENTURIO SDD detector.

Nanoparticle tracking analysis: NTA analyses were performed at 25 °C using a NanoSight LM10 (Malvern Instruments, Ltd, UK) instrument equipped with an sCMOS camera. Samples

were prepared by NP dispersion in ultrapure Milli-Q water (50 mg/L). Measurement of each sample was performed in triplicate, consisting of three records of 60 s. The results are presented as the mean size of the particles ± SD. NTA is known to provide accurate measurements even for polydisperse nanoparticles and was thus used without any complementary measurement by dynamic light scattering measurements.

Fluorescence measurement: Fluorescence spectra were acquired with a Fluorolog-3-2iHR320 modular spectrofluorometer (HORIBA Jobin Yvon SAS, Palaiseau, France). The standard light source of the fluorimeter was substituted by a 980 nm continuous-wave laser operating at a power of 1.5 W. Emission was collected between 400 nm and 750 nm.

Two-photon microscopy: Samples were imaged on a Zeiss LSM-710 two-photon microscope equipped with a Ti: Sapphire Chameleon Vision II laser (Coherent, Santa Clara, California) operating at 980 nm (4% of max power for UCNPs and 50% for µ-Blank-PE and µ-Upcon-PE samples, 140 fs pulses, 80 MHz repetition rate) and a Zeiss Plan-Apochromat 63x/1.40 oil immersion lens. Upconverted light was collected between 490 and 600 nm for the green band and 630 and 710 nm for the red band. Images were processed using ImageJ (Fiji) software.

Zeta-potential measurements: Zeta-potential measurements for MPs and NPs were carried out at 25 °C on a Zetasizer Nano-ZS (Malvern Instruments, Ltd, UK) equipped with a He-Ne laser (λ = 633 nm) at an angle of 173°. Samples were prepared by dispersion of particles in 10 mM NaCl solution to provide a minimum level of conductivity in the samples, following ISO and ASTM standard guides. Before analysis, the pH of every sample was measured. The zeta potential and standard deviation (SD) were obtained from 5 measurements of 11 runs of 10 seconds using the Smoluchowski model.

Results

Large-scale monodisperse UCNP synthesis

Using classical thermal coprecipitation to prepare hydrophobic oleate-coated $NaREF_4$ UCNPs, we implemented a new protocol to achieve the synthesis of monodisperse 20 nm UCNPs over a multigram scale. This approach allows the use of a single batch of phosphors to be further dispatched in multiple assays, therefore maintaining a homogeneous luminescence response over all samples. [31, 32] As we noticed that a slow and separate introduction of fluoride and sodium sources via syringe pumps to the rare earth oleate mixture led to a dramatic size reduction, [33] we decided to adapt this strategy to the efficient protocol described by Zhang et al., known to yield 40 nm $NaYF_4$-based UCNPs.[34] W collected regular hexagonal prism-shaped erbium-doped $NaYF_4$:$Yb_{30\%}$ and $Er_{2\%}$ UCNPs ($NaREF_4$, where RE= 2% Er; 30% Yb; 68% Y) with an average size of 21.8±1.3 nm even on an 11.6 mmol scale: up to 3 g of bright green emissive UCNPs could be obtained in this way. XRD analysis was consistent with the pure hexagonal phase (Figure 1).

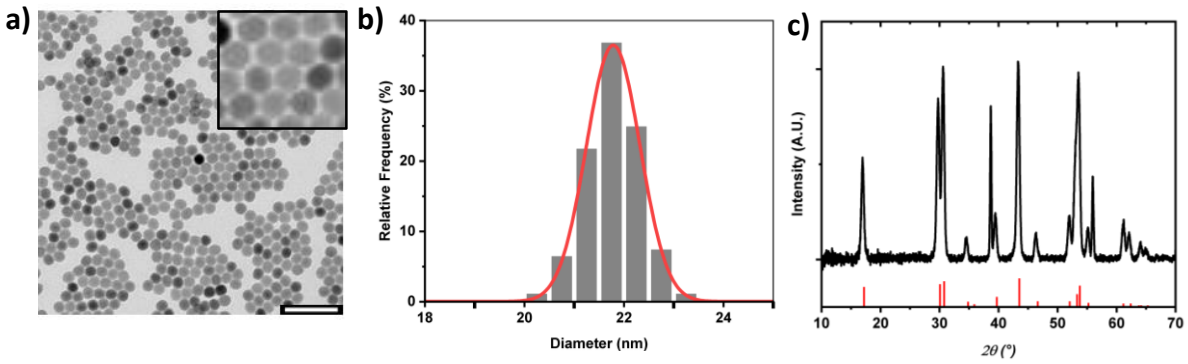

Figure 1. Transmission electron microscopy (TEM) and X-ray diffraction characterization of the prepared $NaYF_4$:$Yb_{30\%}$,$Er_{2\%}$, A: TEM image (scale bar is 100 nm). B: Size distribution obtained from analysis of TEM images (Gaussian fit in red). C: XRD diffractogram of the particles (red lines show the characteristic peaks of hexagonal $NaYF_4$ (JCPDS 00-016-0334)).

Incorporation of UCNP in PE and powdering

241 We chose to incorporate UCNPs into the polymer using a dissolution/precipitation procedure,
242 which allows one to work on smaller quantities than melt mixing (**Figure 2a**). The UCNP:PE
243 ratio was chosen by comparison with a standard nanocomposite formulation involving
244 HDPE.[35] Briefly, PE was solubilized in boiling o-xylene in the presence of UCNPs (10% in
245 weight). Cooling the colorless solution at 0 °C led to the quantitative precipitation of the
246 polymer. Excitation of the collected whitish solid with a 976 nm continuous-wave (CW) laser
247 induced the bright green luminescence typical of Er^{3+}, indicating that UCNPs were successfully
248 incorporated in bulk PE (Upcon-PE). A similar test was found to be negative for UCNP-free
249 synthesis, Blank-PE.
250 The powdering process consisted of a first step to cryogenic grinding. We selected this method
251 because it is a process where thermally sensitive and elastic substances are generally
252 successfully processed. The effect of several parameters was considered, including precooling
253 time, grinding time, and oscillation frequency. Experiments reveal a nonmonotonous effect of
254 these parameters on abrasion efficiency. At this stage of the powdering process, particles at
255 the nanoscale were not detected by nanoparticle tracking analysis (NTA). Both powders, with
256 or without UCNPs, were named μ-Upcon-PE and μ-Blank-PE, respectively. The size distribution
257 obtained by granulometric analysis showed that approximately 90% of the particles were
258 smaller than 15 μm (**Figure 2b**). The incorporation of the UCNPs did not significantly impact
259 the size distribution of the powder (**Figure S1**).
260 To reach the nanoscale, we proceeded to further size reduction using a low-energy wet-driven
261 milling technique. The method is simple, economical, sustainable and, similar to the first step,
262 provides the advantage of the preservation of the polymer structure.[36] It consists of preparing
263 a dispersion of the powder in a solvent, adding zirconium beads and then slowly rolling the
264 solution. Ethanol was chosen as the solvent because synthesis in water, which would be more

appropriate for future use in toxicological tests, was not possible. PE is very hydrophobic and does not wet in water. Furthermore, PE floating in water and contact with zirconium beads used for milling were not favored. After the two-stage powdering process, the particles were fractionated by sequential filtration in ethanol (using a 6 mesh cutoff: 500 µm, 200 µm, 100 µm, 50 µm, 11 µm, and 1 µm). This easy-to-implement protocol is aimed at preventing rapid clogging of the filter mesh during filtration without resorting to a more complex process, such as tangential flow filtration (TFF).[37] Nanoscale particles (nano-Upcon-PE and nanoblank-PE) were produced with a yield of approximately 6%. The distribution of the particles by nanoparticle tracking analysis (NTA) showed that approximately 90% of the particles were smaller than 201 nm for nanoblank-PE and 117 nm for nano-Upcon-PE (**Figure 2c** or **Figure SI2** for details). The incorporation of UCNPs led to smaller particles; we have no explanation for this result.

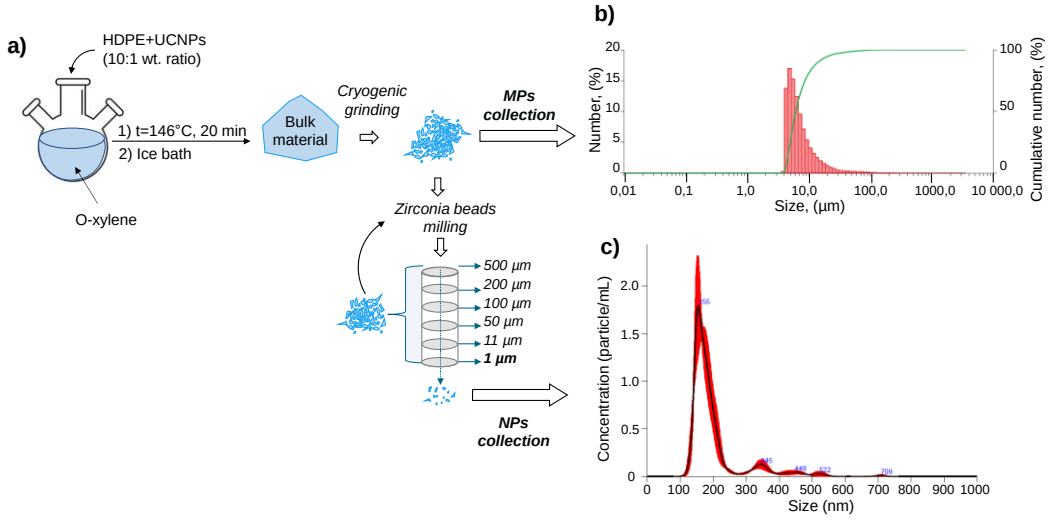

Figure 2. a) General scheme of upconverting nanoparticles (UCNPs) incorporated into polyethylene (PE) followed by a two-step powdering process to prepare micro- and nanometric particles. b) Granulometric analysis of the micrometric fraction obtained after cryogenic grinding, expressed as a percentage and cumulative percentage as a function of size. c) Nanoparticle tracking analysis (NTA) of the nanometric fraction obtained after wet milling and cascade filtration.

Characterization of labelled micro- and nanoplastics

Chemical integrity of PE

Attenuated total reflection Fourier transform infrared (ATR-FTIR) analysis of the samples (on bulk, micrometric and nanometric particles) was performed to determine if any PE degradation occurred during synthesis or powdering. An important side reaction could be PE oxidation leading, in particular, to the formation of carbonyl moieties, which is easily detected by an intense absorption band in the region of 1650–1850 cm^{-1}.[38] FTIR spectra were obtained after each processing step and compared to the spectra of raw PE pellets. No absorption band due to the presence of oxidation was detected (**Figure S3**). This result indicates that synthesis and grinding processes do not cause any chemical modification of PE.

Effectiveness of UCNPs incorporation in PE

During the synthesis of the bulk material, the dissolution/precipitation procedure does not allow control of the UCNP rate of incorporation. This amount was measured by two distinct techniques: differential scanning calorimetry (DSC) and thermogravimetric analysis (TGA). DSC was used to accurately determine the PE crystallinity at each stage of the preparation. The melting enthalpy (ΔH_m), onset temperature (T_{onset}), and exothermic peak temperature (T_{peak}) of crystallization were obtained from the second heating cycle (Table 1). If a polymer is mixed with a material that does not melt in the same temperature range, DSC is a way to record in what proportion it is added.[35] We selected the second cycle because this measurement does not record the history of the material, such as the way it was cooled (however, the use of the enthalpy recorded at the first cycle gave the same proportion of incorporated UCNPs, data not shown).

The melting points were similar regardless of the stage of the process; this result confirms the absence of PE chemical modification after the incorporation of UCNPs or powdering. Before engagement in the dissolution/precipitation step, the PE raw pellet and raw powder had

similar melting enthalpies. After cryogenic grinding, the enthalpy of µ-Blank-PE was slightly superior, that is, the polymer was slightly more crystalline at this stage (85% crystallinity compared to 83% initially). Knowing that UCNPs are thermodynamically stable in the hexagonal phase up to 700 °C,[39] their presence did not contribute to the enthalpy recorded between 20 °C and 160 °C. This result led us to a UCNP-content in µUpcon-PE of 6.4 ± 1.2 wt.%. This rate was confirmed by thermogravimetric analysis, which gave a value of 5.7% (Table S1).

Table 1. DSC analysis of raw PE pellets, µ-Blank-PE and µ-Upcon-PE. The melting enthalpy, onset temperature and exothermic peak temperature were obtained from the second heating cycle (average values ± SD). The corresponding degrees of crystallinity (X_c) were calculated as the ratio between ΔH_m of the sample and the reference ΔH_{mref} value of a 100% crystalline form of PE (293 J g^{-1}).[37,38]

Sample	ΔH_m, (J g^{-1})	T_{onset}, (°C)	T_m, (°C)	X_c, (%)
PE raw pellet	-243.7 ± 1.4	122.4 ± 0.1	128.3 ± 0.4	83.2 ± 0.5
PE raw powder	-244.2 ± 3.4	122.8 ± 0.2	128.5 ± 0.3	83.3 ± 1.2
µ-Blank-PE	-250.6 ± 2.9	122.2 ± 0.1	128.9 ± 0.2	85.5 ± 1.0
µ-Upcon-PE	-234.5 ± 1.5	122.4 ± 0.3	129.2 ± 0.3	

Study of UCNPs dispersion within PE

The way UCNPs were incorporated in PE was investigated in detail with particles at the microscale by small-angle X-ray scattering (SAXS). Details of the applied models for SAXS are given in the Supporting Information. The SAXS curve of µ-Blank-PE (**Figure 3a** and **Figure S4**) shows a constant decay with a small inflection of approximately 0.05 $Å^{-1}$, reflecting the correlation distance between crystalline parts present in the PE matrix. The SAXS curve of µ-Upcon-PE follows the same decay as the SAXS curve of µ-Blank-PE plus the contribution of UCNPs (**Figure 2a**). The first result confirms that the UCNPs do not alter the organization of

PE. The contribution of UCNPs was investigated to depict whether the UCNPs were either adsorbed on the surface or only partially incorporated into PE. To discriminate the last case, a simulated SAXS curve was obtained by a linear combination of the two contributions and compared to the experimental curve (**Figure 3b**). Data were plotted in Log I(q)×q^4 as a function of Log q to magnify the differences. No linear combination of the SAXS curves of PE and UCNPs was found to fit the experimental SAXS data of Upcon-PE. The difference observed between the curves suggests that another term contributes to the SAXS curves. In the case where UCNPs are distributed in the PE matrix, it is necessary to consider the scattering cross terms, which reflect the interactions between atoms of UCNPs and PE. A simplified model was applied to describe μ-Upcon-PE, and a two-component model was applied to describe the organization at large distances (see "Applied models for SAXS analysis" and **Figure S5** in the Supporting Information for more details). The states of the surfaces of μ-Blank-PE and μ-Upcon-PE were found to be similar, indicating that the incorporation of UCNPs does not induce any modification of the surface particle properties. This inference suggests that UCNPs are not adsorbed onto the surface of PE but rather fully incorporated inside the PE matrix. This result is interesting since PE is not prone to easily accept the incorporation of other materials, and fabrication of PE composites generally requires a more complex process than a simple dissolution/precipitation procedure such as the one proposed here.[40, 41] The effective incorporation of UCNPs into PE prevents UCNPs from leaching and enables their detectability regardless of the treatments or experiments performed (washing, purification, use in vivo, etc.).

a) b)

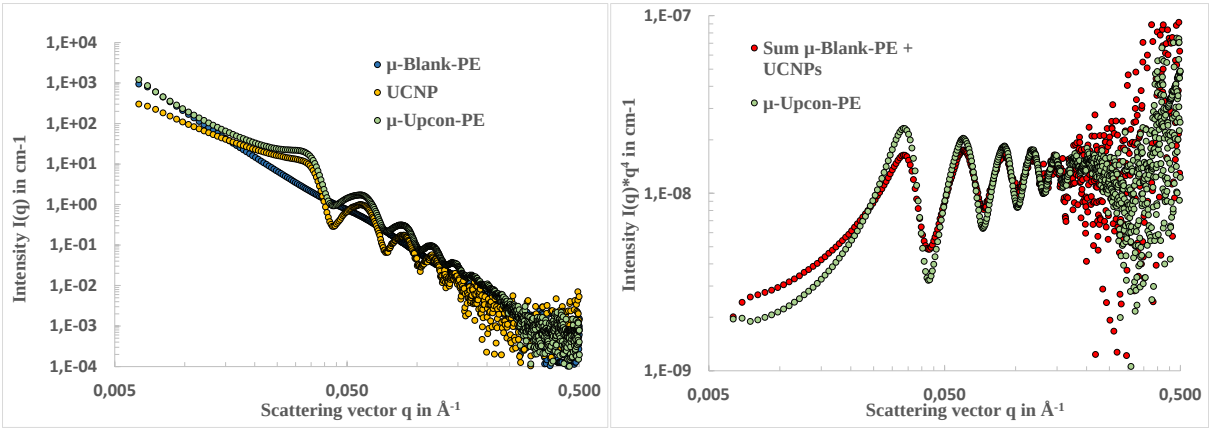

Figure 3. Small-angle X-ray scattering (SAXS) analysis of a) µ-Blank-PE (blue curve), µ-Upcon-PE (green curve) and UCNPs alone (yellow curve), where Log I(q) is plotted as a function of Log q; b) µ-Upcon-PE spectrum and a simulated spectrum of a linear combination of the scattering curves of µ-Blank-PE and UCNPs, considered two independent contributions; Log I(q)×q^4 is plotted as a function of Log q.

Colloidal properties of labelled nanoplastics

Electron microscopy

As discussed earlier, NTA allowed us to conclude that the particles prepared at the nanoscale were very polydisperse and mostly smaller than 200 nm. The shape of the particles was assessed by electron microscopy (TEM) and showed that the particles were indeed polydisperse and polymorphic (**Figure 4a**). The incorporation of UCNPs did not modify their shapes (data not shown). The heterogeneous shapes obtained by this top-down process are in accordance with a recent study. [42] The darker dots in the particles were supposed to be UCNPs because they were expected to be highly dense, and their size was approximately 20 nm (Figure 4a). The images showed that the UCNPs were rather well dispersed within PE particles. The identification of UCNPs was confirmed by high-resolution TEM coupled to energy-dispersive X-ray elemental analysis (TEM-EDX), as the dark dots showed the homogeneous distribution of F, Y and Yb (see **Figure 4 b** and **Figure S6** for more details). This

result showed that the chemical integrity of UCNPs was maintained during the powdering process, as well as their sizes and shapes.

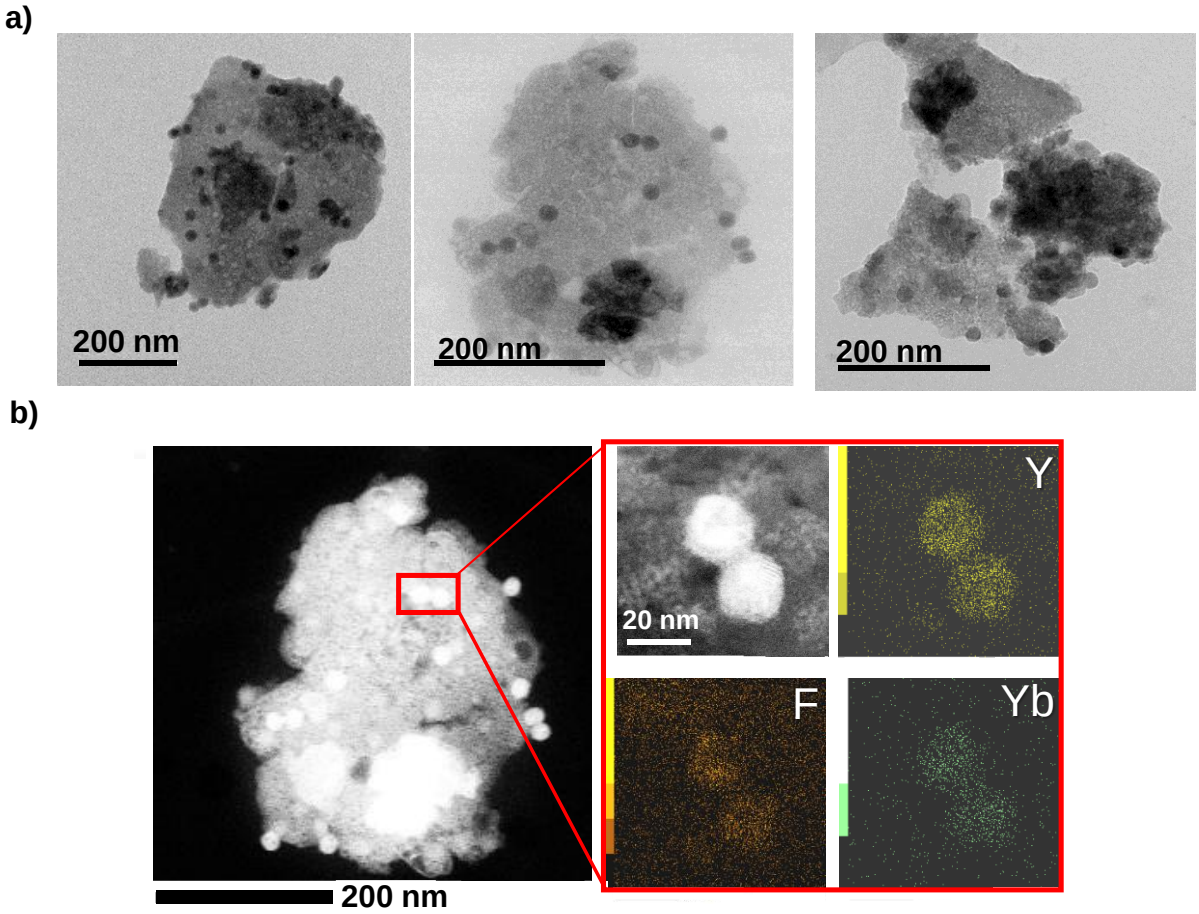

Figure 4. a) Transmission electron microscopy (TEM) bright-field images of nano-Upcon-PE. The three images illustrate that the particles were polydisperse and polymorphic. b) High-angle annular dark-field (HAADF) TEM of a single nano-Upcon-PE, along with energy-dispersive X-ray characterization of yttrium (Y), fluorine (F) and ytterbium (Yb).

Zeta potential

The surface charge of the produced micro- and nanometric particles was obtained by zeta-potential (ζ-potential) measurements. At the micro- and nanoscales, the particles were found to be negatively charged (Table S2). The presence of incorporated UCNPs did not significantly modify the particle charges. The zeta potentials for the micro- and nanometric particles were approximately -70 mV and -60 mV, respectively. These values were in accordance with a

recent study using the top-down process; all the model NPs were negatively charged, and those in PE had a zeta potential of -38 ±2.4 mV at a similar pH.[42]

It is expected that most NP surfaces would bear functional groups such as carboxylic acids or hydroxyl groups resulting from the oxidation of the polymer; consequently, at neutral pH, they are expected to be negatively charged. The model NPs prepared are also negatively charged. This parameter is important, as the surface charge of nanoparticles dramatically affects their behavior in the environment or in vivo.[43]

Emission properties of labeled nanoplastics

The emission properties of the UCNPs once incorporated in PE were investigated. Fluorescence measurements ($\lambda_{exc.}$ = 980 nm) of the dispersed particles in ethanol showed no emission for Blank-PE, while Upcon-PE showed three emission peaks at approximately 525, 550 and 655 nm, attributed to the Er^{3+} transitions $^2H_{11/2} \rightarrow {}^4I_{15/2}$, $^4S_{3/2} \rightarrow {}^4I_{15/2}$ and $^4F_{9/2} \rightarrow {}^4I_{15/2}$.[33]. These specific emission peaks were observed with µ-Upcon-PE and nano-Upcon-PE (**Figure 5**).

To check whether the UCNPs maintained their functionality once encapsulated in PE, the emission properties of all the prepared particles were investigated under upconversion conditions. Under continuous-wave laser irradiation at 980 nm, the pristine Er-UCNPs displayed typical green visible luminescence. The recorded spectrum of the dispersed UCNPs in cyclohexane showed three emission peaks at approximately 525, 550 (green) and 655 nm (red), attributed to the Er^{3+} transitions $^2H_{11/2} \rightarrow {}^4I_{15/2}$, $^4S_{3/2} \rightarrow {}^4I_{15/2}$ and $^4F_{9/2} \rightarrow {}^4I_{15/2}$, respectively. [33] (**Figure 5**). As expected, blank PE particles dispersed in ethanol did not show any signal in this spectral range upon excitation under similar conditions. However, Upcon-PE (micro- and nanoscale) displayed an emission spectrum similar to that of UCNPs: the upconversion property was not lost in the PE incorporation/grinding and milling process.

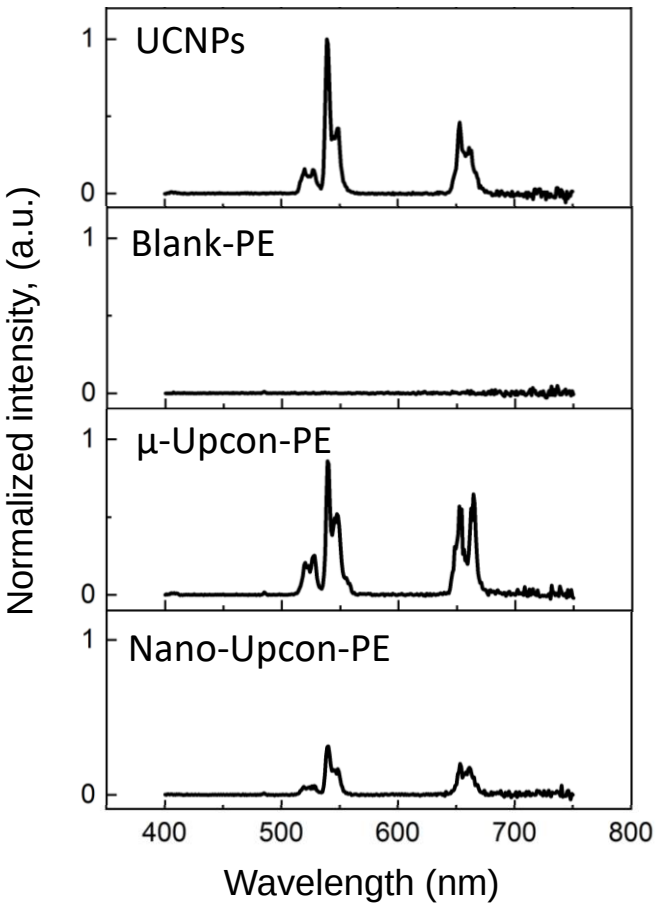

Figure 5. Upconversion emission spectra of UNCPs, Blank-PE, and Upcon-PE micro- and nanoparticles; normalized fluorescence intensity as a function of the wavelength ($\lambda_{exc.}$ = 980 nm). Acronyms: lanthanide-based upconverting nanophosphors (UCNPs), polyethylene (PE), raw PE (Blank-PE), UCNP-doped PE particles prepared at the microscale (μ-Upcon-PE), UCNP-doped PE particles prepared at the nanoscale (nano-Upcon-PE).

The suitability of these labeled PE particles for imaging purposes was then examined. UCNPs are known to be able to produce an upconversion spectrum under a large range of laser fluences; therefore, a standard 2-photon emission microscope setup was employed. To achieve our goal, the particles were spread over a microscope blade and examined under standard 2-photon microscopy conditions using NIR pulsed laser light. Images showed Z-projection in a maximum intensity. Under these conditions, control particles (μ-Blank-PE) remained nonemissive, while particles of μ-Upcon-PE gave rise to green (G) and red (R)

upconverted light that could be collected between 490 and 600 nm and 630 and 710 nm, respectively. The absence of any emission from the blank PE particle indicates that no 2-photon processes occur in pure PE and justifies the use of UCNPs as a background-free luminescent tag for plastic particles. The band ratio G/R was found differ from that recorded at lower fluence. It is known that the power dependence of the emission lines is rather nonlinear; therefore, the band ratio typically observed at very low fluence, such as with a CW 980 nm laser, can be different when using a more intense pulse laser, which is commonly used to trigger 2-photon fluorescence emission. This spectral alteration is also a signature of the presence of UCNPs and can be used to identify tagged particles in more complex environments.

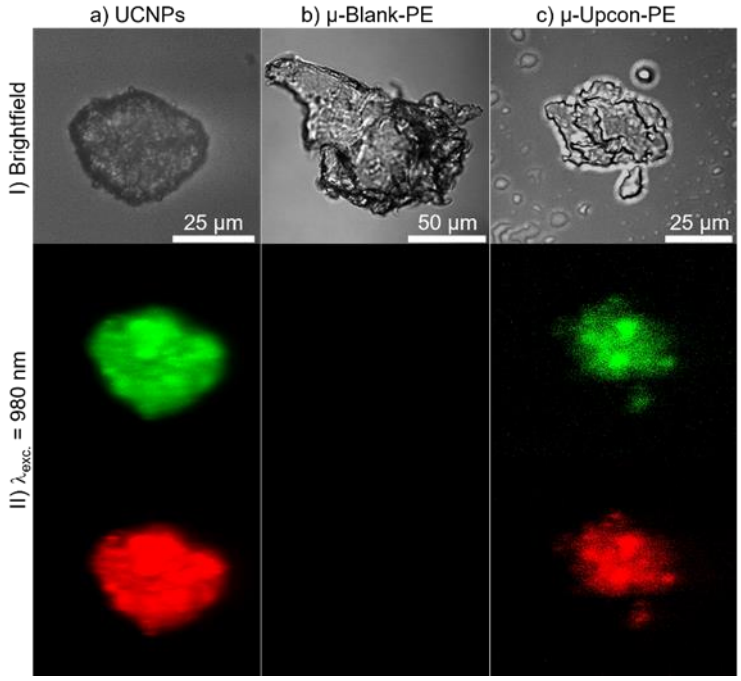

Figure 6. I) Bright-field image of particle aggregates: a) UCNPs; b) µ-Blank-PE; c) µUCNPs-PE. II) Green and red emission under an NIR irradiation observer for a) UCNPs and c) µUCNPs-PE; b) µ-Blank-PE remains nonemissive.

Conclusion

This top-down synthesis allows the production of model plastic particles within the micro- and nanometric range, which present heterogeneity in size and shape that is absent for most of the particles formed by the bottom-up approaches. This method does not allow us to control the amount of UCNPs incorporated in the polymer, as the parameters of the precipitation process are difficult to control, but the UCNP content reaches 6% by weight. Using a series of physicochemical characterizations, we demonstrated that the UCNPs were incorporated within the polymer, not localized at its surface (SAXS), and well dispersed (TEM-EDX). The powdering process does not alter the chemical structure or the morphology of the polymer (ATR-FTIR and DSC). The mixture of micro- and nanometric objects formed can easily be separated by filtration; thus, a range of sizes can be selected for a given application. The nanometric particles were formed in a small proportion (6% yield), but the remaining micrometric particles can be engaged in another long process of wet milling for further production of smaller particles.

The incorporation of the UCNPs did not alter their luminescent properties, and the labeled PE particles could be easily monitored with a standard two-photon microscope. This feature offers the possibility to easily detect these model NPs in complex organic matrices, while the detection of plastic itself is always difficult.

The proposed method is compatible with a large variety of polymers, while the UCNP rate of incorporation in the polymer matrix is not easily controllable and certainly depends on the polarity and affinity of the UCNPs for the polymer. However, this method also offers the possibility to use formulated polymers, such as commercialized plastic, to produce plastic particles even closer to those present in the environment. This process is also compatible with weathered polymers.

The prepared particles are very good environmentally relevant models because of their polydispersity and heterogeneity. These two properties are very scarcely considered in actual toxicological evaluation studies because most of the particles used are produced with a bottom-up method.[10] Because of the extreme photostable and NIR-activable luminescent properties of the prepared particles, strategies based on their use can pave the way for a deeper understanding of the fate of plastic particles in the trophic chain.

Acknowledgments

The authors acknowledge the Université Paul Sabatier and CNRS for financial support. C. C., B. A. and A.-F. M. gratefully acknowledge the Agence Nationale de la Recherche (Grant ANR-15-CE09-0020 BLINK) for financial support. We would like to thank Teresa Hungria (The Raimond Castaing Microcharacterization Centre) for the TEM/EDX images, Corinne Routaboul (The Infrared Spectroscopy Service, Institute of Chemistry of Toulouse (ICT)) for help with ATR-FTIR analysis, Rodica Chiriac (Thermal Analysis Platform (PLAT)) at the Laboratory of Multimaterials and Interfaces (LMI) for the TGA analysis, and Christine Rey-Rouch (Service Analyze et Procédés - SAP, Chemical Engineering Laboratory (LGC)) for granulometry analysis.

References

1. O. S. Alimi, J. Farner Budarz, L. M. Hernandez and N. Tufenkji, Microplastics and Nanoplastics in Aquatic Environments: Aggregation, Deposition, and Enhanced Contaminant Transport, *Environ Sci Technol*, 2018, **52**, 1704-1724.
2. J. Gigault, A. ter Halle, M. Baudrimont, P. Y. Pascal, F. Gauffre, T. L. Phi, H. El Hadri, B. Grassl and S. Reynaud, Current opinion: What is a nanoplastic?, *Environ. Pollut.*, 2018, **235**, 1030-1034.
3. A. Ter Halle, L. Jeanneau, M. Martignac, E. Jarde, B. Pedrono, L. Brach and J. Gigault, Nanoplastic in the North Atlantic Subtropical Gyre, *Environ. Sci. Technol.*, 2017, **51**, 13689-13697.
4. A. A. Horton, A. Walton, D. J. Spurgeon, E. Lahive and C. Svendsen, Microplastics in freshwater and terrestrial environments: Evaluating the current understanding to

identify the knowledge gaps and future research priorities, *Sci. Total Environ.*, 2017, **586**, 127-141.
5. M. Cole, P. Lindeque, E. Fileman, C. Halsband, R. Goodhead, J. Moger and T. S. Galloway, Microplastic Ingestion by Zooplankton, *Environ. Sci. Technol.*, 2013, **47**, 6646-6655.
6. L. J. Zantis, E. L. Carroll, S. E. Nelms and T. Bosker, Marine mammals and microplastics: A systematic review and call for standardisation, *Environ. Pollut.*, 2021, **269**, 116142.
7. S. Anbumani and P. Kakkar, Ecotoxicological effects of microplastics on biota: a review, *Environ Sci Pollut Res Int*, 2018, **25**, 14373-14396.
8. C. G. Alimba and C. Faggio, Microplastics in the marine environment: Current trends in environmental pollution and mechanisms of toxicological profile, *Environ. Toxicol. Pharmacol.*, 2019, **68**, 61-74.
9. T. S. Galloway, M. Cole and C. Lewis, Interactions of microplastic debris throughout the marine ecosystem, *Nat Ecol Evol*, 2017, **1**.
10. J. Gigault, H. El Hadri, B. Nguyen, B. Grassl, L. Rowenczyk, N. Tufenkji, S. Y. Feng and M. Wiesner, Nanoplastics are neither microplastics nor engineered nanoparticles, *Nat. Nanotechnol.*, 2021, **16**, 501-507.
11. C. Larue, G. Sarret, H. Castillo-Michel and A. E. P. del Real, A Critical Review on the Impacts of Nanoplastics and Microplastics on Aquatic and Terrestrial Photosynthetic Organisms, *Small*, **17**, 2005834.
12. L. C. de Sa, M. Oliveira, F. Ribeiro, T. L. Rocha and M. N. Futter, Studies of the effects of microplastics on aquatic organisms: What do we know and where should we focus our efforts in the future?, *Sci. Total Environ.*, 2018, **645**, 1029-1039.
13. A. P. Reverberi, M. Vocciante, E. Lunghi, L. Pietrelli and B. Fabiano, New trends in the synthesis of nanoparticles by green methods, *Chem. Eng. Trans.*, 2017, **61**, 667-672.
14. D. Magri, P. Sanchez-Moreno, G. Caputo, F. Gatto, M. Veronesi, G. Bardi, T. Catelani, D. Guarnieri, A. Athanassiou, P. P. Pompa and D. Fragouli, Laser Ablation as a Versatile Tool To Mimic Polyethylene Terephthalate Nanoplastic Pollutants: Characterization and Toxicology Assessment, *Acs Nano*, 2018, **12**, 7690-7700.
15. A. F. Astner, D. G. Hayes, H. O'Neill, B. R. Evans, S. V. Pingali, V. S. Urban and T. M. Young, Mechanical formation of micro- and nano-plastic materials for environmental studies in agricultural ecosystems, *Sci. Total Environ.*, 2019, **685**, 1097-1106.
16. H. El Hadri, J. M. Lisa, J. Gigault, S. Reynaud and B. Grassl, Fate of nanoplastics in the environment: Implication of the cigarette butts, *Environ. Pollut.*, 2021, **268**.
17. M. Baudrimont, A. Arini, C. Guegan, Z. Venel, J. Gigault, B. Pedrono, J. Prunier, L. Maurice, A. Ter Halle and A. Feurtet-Mazel, Ecotoxicity of polyethylene nanoplastics from the North Atlantic oceanic gyre on freshwater and marine organisms (microalgae and filter-feeding bivalves), *Environ. Sci. Pollut. R.*, 2020, **27**, 3746-3755.
18. M. Sander, H. E. Kohler and K. McNeill, Assessing the environmental transformation of nanoplastic through (13)C-labelled polymers, *Nat. Nanotechnol.*, 2019, **14**, 301-303.
19. D. M. Mitrano, A. Beltzung, S. Frehland, M. Schmiedgruber, A. Cingolani and F. Schmidt, Synthesis of metal-doped nanoplastics and their utility to investigate fate and behaviour in complex environmental systems, *Nat. Nanotechnol.*, 2019, **14**, 362-368.
20. T. Maes, R. Jessop, N. Wellner, K. Haupt and A. G. Mayes, A rapid-screening approach to detect and quantify microplastics based on fluorescent tagging with Nile Red, *Sci. Rep.*, 2017, **7**, 44501.

21. A. Paganin-Gioanni, E. Bellard, L. Paquereau, V. Ecochard, M. Golzio and J. Teissie, Fluorescence imaging agents in cancerology, *Radiol. Oncol.*, 2010, **44**, 142-148.
22. P. Greenspan and S. D. Fowler, Spectrofluorometric studies of the lipid probe, nile red, *J. Lipid Res.*, 1985, **26**, 781-789.
23. S. F. Himmelstoss and T. Hirsch, A critical comparison of lanthanide based upconversion nanoparticles to fluorescent proteins, semiconductor quantum dots, and carbon dots for use in optical sensing and imaging, *Methods Appl Fluoresc*, 2019, **7**, 022002.
24. M. Kermorgant, J. Ben Salem, J. Santelli, D. Calise, A. C. Oster, O. Lairez, C. Coudret, M. Verelst, C. Gales, J. M. Senard, F. Beaudry, A. Pavy-Le Traon, C. Roux, R. Mauricot and D. N. Arvanitis, Evaluation of upconverting nanoparticles towards heart theranostics, *Plos One*, 2019, **14**, e0225729.
25. B. Amouroux, C. Roux, J. C. Micheau, F. Gauffre and C. Coudret, A photochemical determination of luminescence efficiency of upconverting nanoparticles, *Beilstein J. Org. Chem.*, 2019, **15**, 2671-2677.
26. M. V. DaCosta, S. Doughan, Y. Han and U. J. Krull, Lanthanide upconversion nanoparticles and applications in bioassays and bioimaging: a review, *Anal. Chim. Acta*, 2014, **832**, 1-33.
27. Y. I. Park, K. T. Lee, Y. D. Suh and T. Hyeon, Upconverting nanoparticles: a versatile platform for wide-field two-photon microscopy and multi-modal in vivo imaging, *Chem. Soc. Rev.*, 2015, **44**, 1302-1317.
28. Yang R., *Principles and application of up-converting phosphor technology*, 2019.
29. D. Kang, E. Jeon, S. Kim and J. Lee, Lanthanide-doped upconversion nanomaterials: recent advances and applications, *BioChip Journal*, 2020, **14**, 124-135.
30. S. Wu, G. Han, D. J. Milliron, S. Aloni, V. Altoe, D. V. Talapin, B. E. Cohen and P. J. Schuck, Non-blinking and photostable upconverted luminescence from single lanthanide-doped nanocrystals, *P. Natl. Acad. Sci. USA*, 2009, **106**, 10917-10921.
31. S. Wilhelm, M. Kaiser, C. Wurth, J. Heiland, C. Carrillo-Carrion, V. Muhr, O. S. Wolfbeis, W. J. Parak, U. Resch-Genger and T. Hirsch, Water dispersible upconverting nanoparticles: effects of surface modification on their luminescence and colloidal stability, *Nanoscale*, 2015, **7**, 1403-1410.
32. Y. R. Jiao, C. Ling, J. X. Wang, H. Amanico, J. Saczek, H. Y. Wang, S. Sridhar, B. B. Xu, S. Wang and D. Wang, Controllable Synthesis of Upconversion Nanophosphors toward Scale-Up Productions, *Particle & Particle Systems Characterization*, 2020, **37**.
33. B. Amouroux, C. Roux, J. D. Marty, M. Pasturel, A. Bouchet, M. Sliwa, O. Leroux, F. Gauffre and C. Coudret, Importance of the Mixing and High-Temperature Heating Steps in the Controlled Thermal Coprecipitation Synthesis of Sub-5-nm Na(Gd-Yb)F4:Tm, *Inorg. Chem.*, 2019, **58**, 5082-5088.
34. Z. Li and Y. Zhang, An efficient and user-friendly method for the synthesis of hexagonal-phase NaYF(4):Yb, Er/Tm nanocrystals with controllable shape and upconversion fluorescence, *Nanotechnology*, 2008, **19**, 345606.
35. J. L. Gao, Y. H. Liu and S. D. Wei, Preparation and Properties of High-Density Polyethylene/Silica Composites, *Advanced Material Research*, 2011, **279**, 115-119.
36. M. Trofa, G. D'Avino, B. Fabiano and M. Vocciante, Nanoparticles Synthesis in Wet-Operating Stirred Media: Investigation on the Grinding Efficiency, *Materials*, 2020, **13**.

37. M. Dehghani, K. Lucas, J. Flax, J. McGrath and T. Gaborski, Tangential flow microfluidics for the capture and release of nanoparticles and extracellular vesicles on conventional and ultrathin membranes, *Adv. Mater. Technol.*, 2019, **4**.
38. E. Chiellini, A. Corti, S. D'Antone and R. Baciu, Oxo-biodegradable carbon backbone polymers - Oxidative degradation of polyethylene under accelerated test conditions, *Polym. Degrad. Stab.*, 2006, **91**, 2739-2747.
39. R. E. Thoma, H. Insley and M. Hebert, The sodium fluoride-lanthanide trifluoride systems, *Inorg. Chem.*, 1966, **5**, 1222-1229.
40. W. H. Xu, Y. He, H. Xie, S. Qin, L. C. Tan, T. Wu and J. P. Qu, Ultrafast Fabrication of Graphene-Reinforced Nanocomposites via Synergy of Steam Explosion and Alternating Convergent-Divergent Flow, *Small*, 2021, **17**, e2100017.
41. C. Hu, X. Liao, Q. H. Qin and G. Wang, The fabrication and characterization of high density polyethylene composites reinforced by carbon nanotube coated carbon fibers, *Compos.-A: Appl. Sci. Manuf.*, 2019, **121**, 149-156.
42. H. El Hadri, J. Gigault, B. Maxit, B. Grassl and S. Reynaud, Nanoplastic from mechanically degraded primary and secondary microplastics for environmental assessments, *Nanoimpact*, 2020, **17**.
43. E. M. Hotze, T. Phenrat and G. V. Lowry, Nanoparticle Aggregation: Challenges to Understanding Transport and Reactivity in the Environment, *J. Environ. Qual.*, 2010, **39**, 1909-1924.

Supporting Information

Top-Down Synthesis of Luminescent Microplastics and Nanoplastics by Incorporation of Upconverting Nanoparticles for Environmental Assessment

Nadiia Yakovenko[a], Baptiste Amouroux[a], Magali Albignac[a], Fabrice Collin[a], Clément Roux[a], Anne-Françoise Mingotaud[a], Pierre Roblin[c], Christophe Coudret[a]*, Alexandra Ter-Halle[a]*

a)

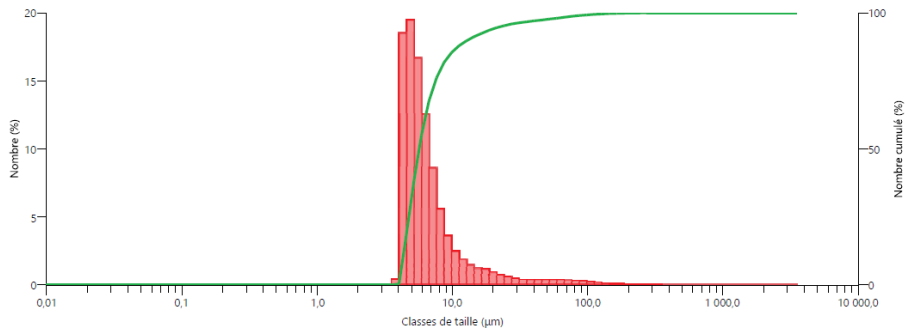

b)

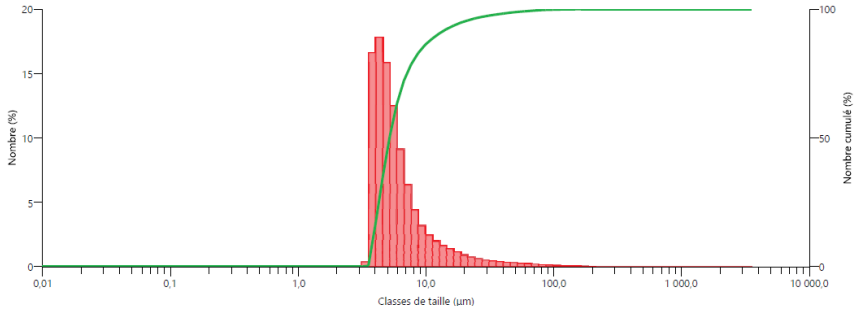

Figure S1. Granulometric analysis after cryogenic grinding, expressed as a percentage and cumulative percentage as a function of the size of a) the blank, where Dn(10)= 4.31 µm, Dn(50)=5.69 µm and Dn(90)=13 µm and b) the UCNP-doped particle, where Dn(10)= 3.82 µm, Dn(50)=5.18 µm and Dn(90)=12.3 µm. The distribution of the particles is not significantly different with or without incorporation of UCNPs. The parameter Dn(x) is the value in the size distribution, up to and including which x% of the total number of particles in the sample is included. Acronyms: upconverting nanoparticles (UCNPs).

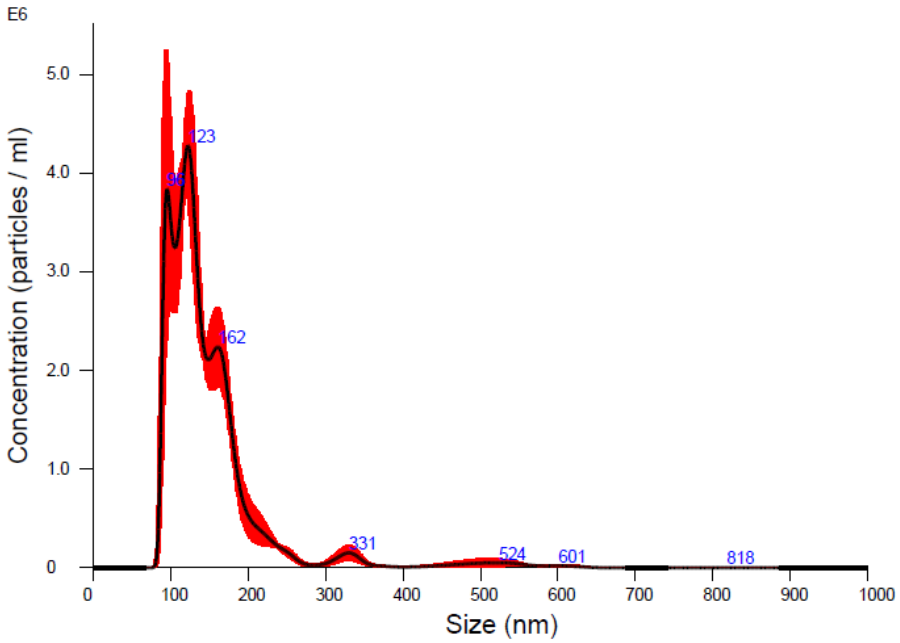

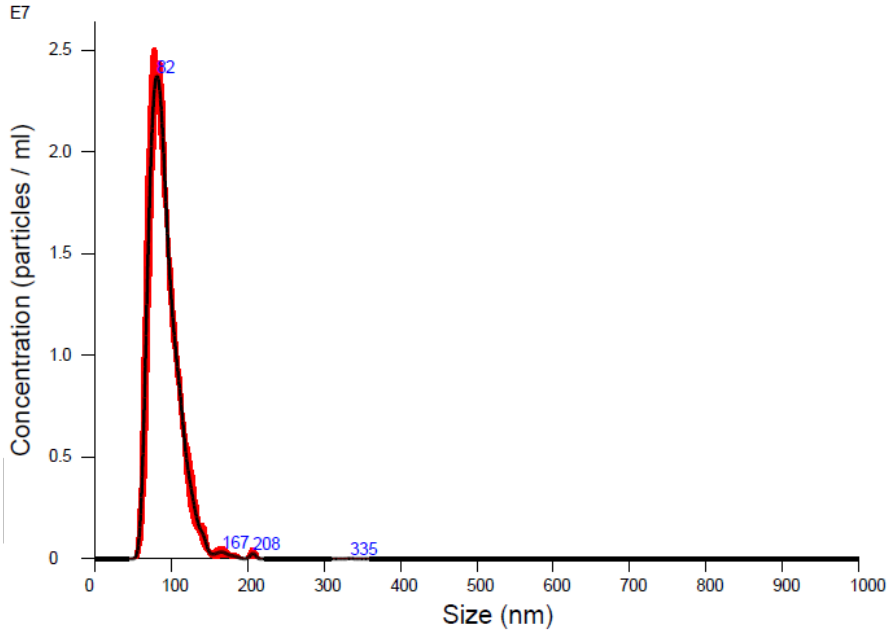

Figure S2. Size distributions of Blank-Upcon-PE and nano-Upcon-PE obtained by nanoparticle tracking analysis (NTA). Data are presented as the average concentration per size over three measurements. For Blank-Upcon-PE, the values obtained were Dn(10)= 96.9 nm, Dn(50)=130.9 nm and Dn(90)=201.4 nm, and b) for nano-Upcon-PE, Dn(10)= 70.8 nm, Dn(50)=87.9 µm and Dn(90)=117.3 nm. The distribution of the particles is not significantly different with or without incorporation of UCNPs. The parameter Dn(x) is the value in the size distribution, up to and including which x% of the total number of particles in the sample is included. Acronyms: upconverting nanoparticles (UCNPs).

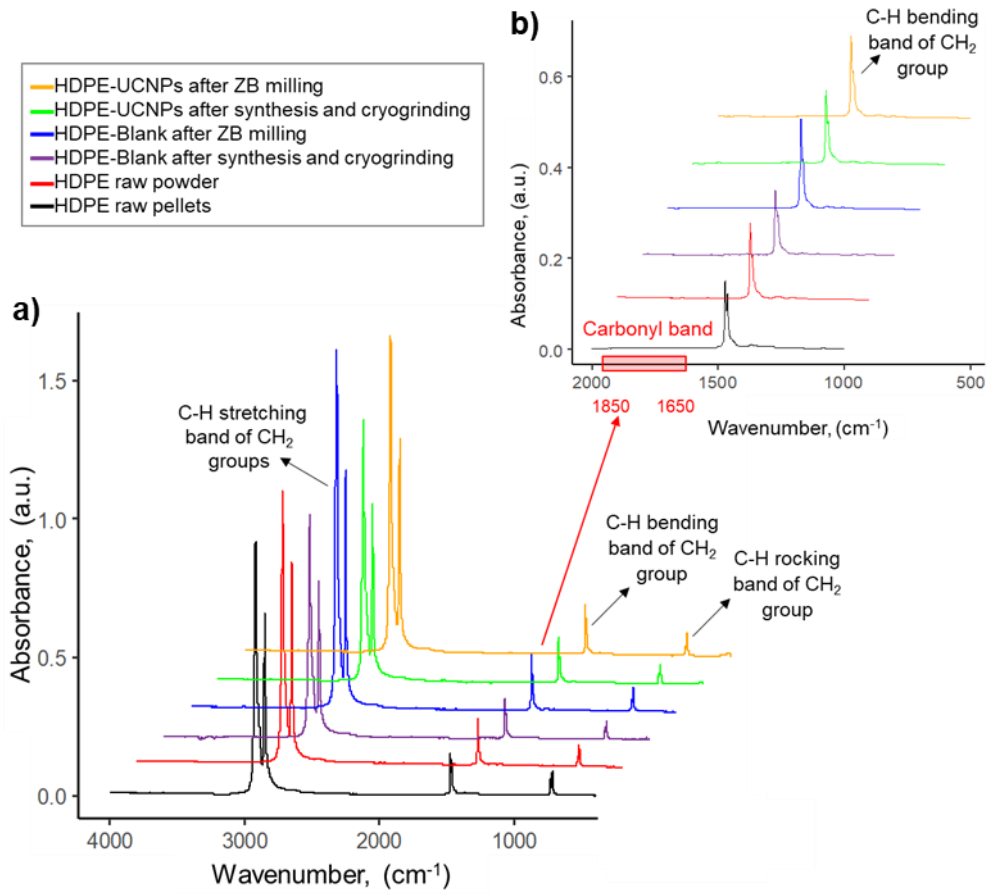

Figure S3. Attenuated total reflectance Fourier transform infrared spectroscopy (ATR-FTIR) of raw PE and at different stages of particle synthesis were recorded using a Thermo Nicolet 6700 spectrometer equipped with a diamond crystal attenuated total reflectance accessory and a deuterated triglycine sulfate (DTGS) detector. Background and sample spectra were recorded as the average of 16 scans in the spectral range of 650–4000 cm^{-1} at a resolution of 4 cm^{-1}. Recorded data were corrected to obtain transmission-like spectra using the ATR Thermo correction (the refractive index considered as 1.5). The carbonyl signal for all analyzed samples was integrated in the 1650-1850 cm^{-1} region. a) FTIR spectra of raw PE material and Blank-PE and Upcon-PE samples recorded after every processing step of MP synthesis (synthesis of bulk material, cryogenic grinding, ZB milling); b) zoom around the carbonyl region, showing the absence of a carbonyl band, which signifies that no oxidation occurs for PE during the synthesis of MPs.

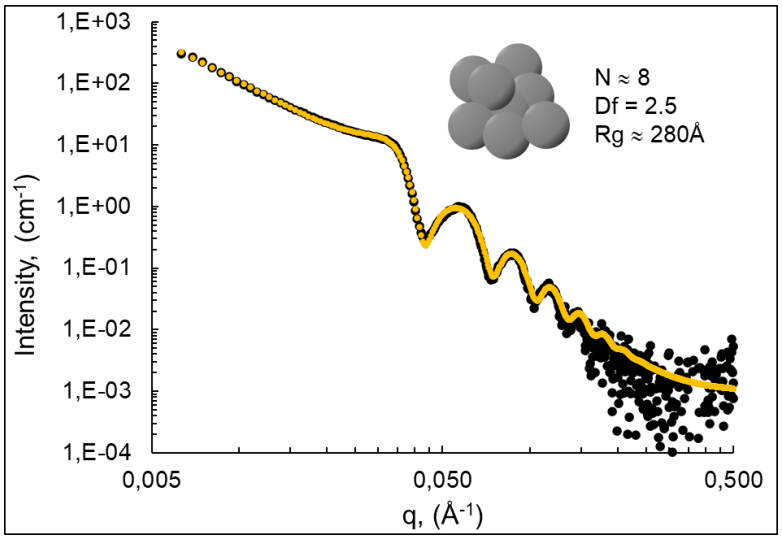

653

654 **Figure S4**: SAXS spectrum of UCNPs in solution. The experimental SAXS curve is plotted in Log
655 I(q) as a function of Log q (black dots). The scattering curve can be described as the scattering
656 of an aggregate object containing hard spheres. The fitting curve corresponding to the
657 modeled SAXS curve is plotted in red dots for a model compatible with the SAXS data that was
658 found to have the following physical parameters: number of nanospheres per cluster N = 8,
659 fractal dimension Df = 2.5 and gyration radius Rg = 280 ± 10 Å.

660

Applied models for SAXS analysis

The SAXS curves can be described by the following equation written with the SASView program (SasView, http://www.sasview.org/):

$$I(q)_{global} = I(q)_{powerlaw} + I(q)_{sphere} * S(q)_{hardsphere} \quad (1)$$

$$I(q)_{global} = Aq^{-P} + \frac{B}{V}\left[\frac{3V(\Delta\rho)(\sin(qr) - qrcos(qr)}{(qr)^3}\right]^2 * S(q)$$

where *A* and B are scaling factors, and the sphere is described by the volume *V*, radius *r* and contrast $\Delta\rho$. The nanospheres interact with each other, and the conditions where *S(q)* = 1 at small angles were not verified. The form factor S(q) is described here with a "hard sphere interaction model" described by Percus-Yevick (J.K. Percus, J. Yevick, J. Phys. Rev., 1958, 110, 1).

When UCNPs are distributed in the PE matrix, the scattering cross terms that reflect the interactions between the atoms of UCNPs and PE must be considered. However, we can apply the simplified model proposed in Equation (1) to describe Upcon-PE and a two-component model to describe the organization of PE MPs at large distances as follows:

$$I(q) = Aq^{-P} + \frac{C}{(1+|q_0-q|\xi)^m} \quad (3)$$

where the second term represents a Lorentzian function to describe the interaction between the crystalline clusters inside the plastic matrix. q_0 is the position of the peak corresponding to the averaged distance separating the clusters (q_0 = 0.05 $Å^{-1}$ ⇔ d = 125 Å).

The most interesting term is the exponential parameter P in Eq. (1) and (3), which describes the state of the particle surface. For both curves, this value is close to 3.7, corresponding to a slightly rough surface. The absence of a difference in the value of P suggests that the presence of UCNPs does not modify the state of the PE MP surface. Thus, these results suggest that UCNPs are absorbed inside the PE matrix.

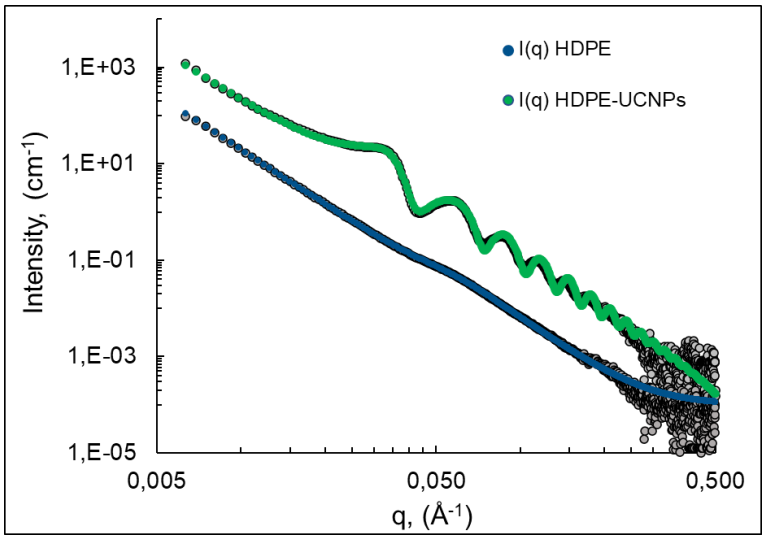

Figure S5. SAXS spectra of Blank-PE and Upcon-PE, along with superimposed fitting curves (blue and green, respectively). The experimental SAXS curves are plotted in Log I(q) as a function of Log q.

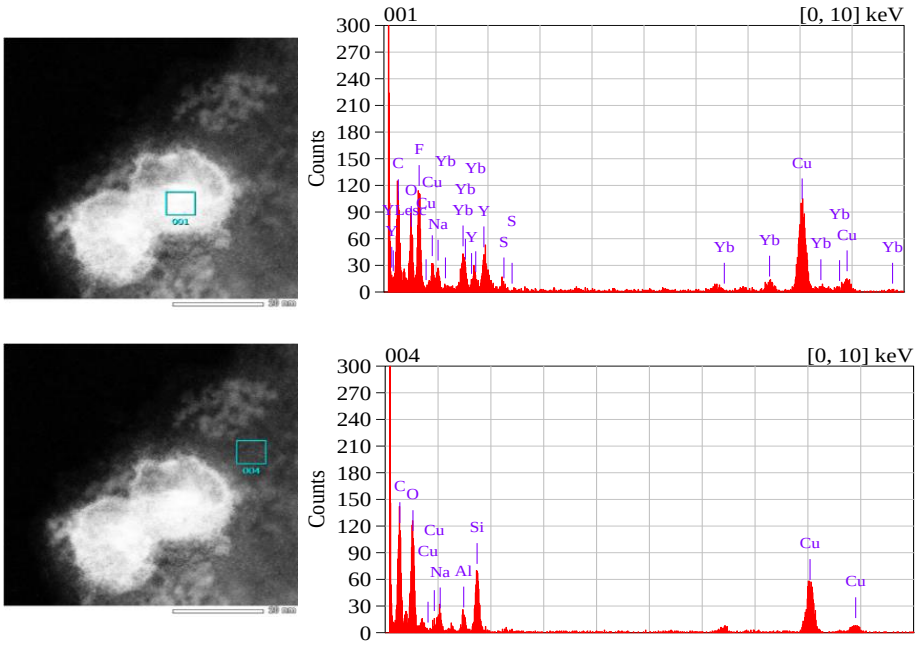

Figure S6. TEM image and energy-dispersive X-ray spectra of Upcon-PE nanoparticles. The box indicates where the measurement was taken on UCNPs (top) and on the PE matrix (bottom). Fluorine, yttrium, and ytterbium were detected in UCNPs but were not present in the PE matrix.

Table S1. The thermal stability of the samples was analyzed using thermogravimetric analysis (TGA). The apparatus was a TGA/SDTA 851 Mettler Toledo device. Approximately 15 mg of each sample was placed in 150 µL aluminum pans with a pierced cover. The analysis was performed from 30 to 900 °C at a heating rate of 10 °C/min under a nitrogen atmosphere with a rated flow of 40 mL/min. For each sample, a blank (analysis with empty crucible) was carried out under the same conditions as for the sample. All samples were analyzed in duplicate.

Sample	Mass, (mg)	T_{peak}, (°C)	Mass loss, (%)	Residue, (%)
PE raw powder	15.31	483	100.8	-0.8
Blank-PE	15.45	483	100.7	-0.7
Upcon-PE	15.84	481	94.3	5.7

Table S2. The average zeta potentials were measured in 10 mM NaCl at a native pH of 7.8 for the micrometric particles and at pH 7.5 for the nanometric particles.

	Zeta potential (mV)
µ-Blank-PE	-71 ± 7
µ-Upcon-PE	-73 ± 8
nano-Blank-PE	-56 ± 11
nano-Upcon-PE	-62 ± 10